Hindawi
Modelling and Simulation in Engineering
Volume 2022, Article ID 3328719, 17 pages
https://doi.org/10.1155/2022/3328719

Research Article

Optimized Luenberger Observer-Based PMSM Sensorless Control by PSO

Rongfu Luo,[1,2] Zenghui Wang,[3] and Yanxia Sun[1]

[1]*Department of Electrical and Electronic Engineering Science, University of Johannesburg, Johannesburg 2006, South Africa*
[2]*Huzhou Yueqiu Motor Co., Ltd., Huzhou 313009, China*
[3]*Department of Electrical Engineering, University of South Africa, Florida 1709, South Africa*

Correspondence should be addressed to Yanxia Sun; sunyanxia@gmail.com

Received 1 June 2022; Revised 22 July 2022; Accepted 27 July 2022; Published 22 August 2022

Academic Editor: Fahad Al Basir

In the real applications, we found that it is difficult to achieve good control performance through manually tuning proportional–integral (PI) parameters of phase locked loop (PLL) and speed-loop of Luenberger observer (LO) for the PMSM sensorless control system. Therefore, this paper is to use the particle swarm optimization (PSO) algorithm to optimize the PI parameters of PLL and speed-loop of Luenberger observer of the system. Firstly, the ranges of PLL parameters are obtained by analyzing the PLL subsystem stability. Then, the ranges of PI parameters of PLL and speed-loop are set based on theoretical estimation and empirical values. The control system model is realized in MATLAB/Simulink that considers the constraints such as the saturation. The integral time absolute error is the objective function, and the PSO with different topologies is used to optimize the PI parameters. The simulation and experimental results show that the proposed method is feasible, and the optimized parameters can effectively improve the precision of position estimation and speed estimation. Moreover, the simulations and experiments are carried out to verify the robustness of the proposed method, and the results show that the optimized system can achieve good performance when there are uncertainties or disturbances.

1. Introduction

The advantages of permanent magnet synchronous motor (PMSM) include high efficiency, high power density, and small size [1–4]. With the development of science and technology, customers, who need higher quality productions and many products, put forward higher requirements for motor control and energy efficiency, which cause the widespread adoption of PMSM in industries like home appliance, industrial engineering, and autoindustry. The field-oriented control (FOC) technology is widely used to control PMSM. In the FOC system, it is necessary to obtain the information of rotor position and speed. In order to obtain the rotor position, some position sensors (such as Hall sensor, photoelectric encoder, and rotary converter) are used to detect the rotor position of the motor. However, the sensor increases the complexity and cost of control systems and reduces the reliability of the system [4]. In order to solve the series of problems caused the position sensors, researchers have proposed the sensorless control technology for PMSM. The research and application of this technology is of great significance and has gradually become one of the hottest fields of motor control, and this kind of control method is called sensorless control [5].

In general, the main methods of sensorless control of PMSM include high frequency injection (HFI), model reference adaptive system (MRAS), flux linkage observer (FLO), extended Kalman filter (EKF), sliding mode observer (SMO), and Luenberger observer (LO). HFI has good control performance on the sensorless low-speed operation [6–8]. However, this method has a poor effect on the recognition of the hidden pole motors besides causing additional noise [9]. MRAS has been used in references [10, 11], but it is dependent on motor parameters excessively [12]. FLO was used in [13, 14], but it has issues of DC offset and harmonics. EKF is good at dynamic performance and anti-interference ability [15, 16], but this algorithm is complex [1, 9]. SMO is simple, and it has good robustness [17–20],

but it has discontinuous switch control, which can cause system chattering [9]. Especially when it runs at low speed, SMO can cause huge torque ripple. LO uses the classical theory of the geometric property of linear (and stationary) systems known as observability [21–23] to estimate the internal states of the system based on the input and output values of the system. It is simple and not chattering and has good robustness [21], but there is division operation in the arctangent function, which can cause larger estimation error of rotor position and speed [19]. It was verified that PLL algorithm can efficiently improve estimation accuracy of rotor position and speed without division operation [2, 20], but it is difficult to tune the PI parameters of PLL [1].

To achieve good control performance of PMSM sensorless control, this paper proposes to use PSO algorithm to optimize PI parameters of PLL and speed-loop. This method can reduce the parameter tuning difficulty and the deviation of PLL and speed-loop effectively, besides improving the speed performance of PMSM sensorless control. The main contributions of this paper are

(1) this study proposed to use PSO algorithm to optimize the PI parameters of PLL and speed-loop of the Luenberger observer-based PMSM sensorless control system, which can reduce the parameters tuning challenges

(2) the optimized PI parameters based on the simulation model of PMSM sensorless control system have been applied to the physical system, and it shows that they can improve the performance of position estimation and speed estimation

(3) simulations and experiments have been used to verify the robustness of the proposed method, and the results show that the optimized system has good performance when there are uncertainties or disturbances

(4) it is found that the random topology of PSO can achieve better performance than the ring topology and global topology

The rest of this paper is arranged as follows. Section 2 gives a brief description of the Luenberger observer-based PMSM sensorless control. A new application for the PSO-optimized PMSM sensorless control system is described in Section 3. In Section 4, the system simulation and experiment are given to verify the performance of the proposed method, and the results are investigated based on some comparisons. Finally, Section 5 gives the conclusion of this study.

2. Luenberger Observer Based on PMSM Sensorless Control System

The PMSM sensorless control system using Luenberger observer is shown in Figure 1. The whole control system is comprised of space vector pulse width modulation (SVPWM), three-phase full bridge inverter circuit, Luenberger observer, and speed and position estimator. The details of Figure 1 are described in the following subsections.

2.1. Mathematical Model of PMSM. This paper uses the stationary stator coordinate system of PMSM as shown in Figure 2. The axes A, B, and C refer to three-phase stationary stator coordinates. Each electric angle is 120°. The axes α and β refer to two-phase stationary stator coordinates. The vector diagram between two-phase stationary stator coordinates and two-phase rotating rotor coordinates is shown as Figure 3. The axes d and q refer to two-phase rotating rotor coordinates. According to rotor field-orientated control, d is the axis where the rotor locates, and the axis q gets ahead 90° of the axis d in an anticlockwise direction. The axis d and q rotate at rotor angular speed ω_r in an anticlockwise direction.

According to Figures 2 and 3, it comes up with the voltage equations that PMSM works under ABC three-phase coordinates.

$$\begin{cases} u_a = Ri_a + \dfrac{d\psi_a}{dt}, \\ u_b = Ri_b + \dfrac{d\psi_b}{dt}, \\ u_c = Ri_c + \dfrac{d\psi_c}{dt}. \end{cases} \tag{1}$$

Here, R is the stator winding resistance; i_a, i_b, and i_c are three-phase current of ABC; u_a,u_b, and u_c are three-phase voltage of ABC; ψ_a, ψ_b, and ψ_c are three-phase stator flux linkage of ABC.

The three-phase stator flux linkage equations of PMSM are

$$\begin{cases} \psi_a = Li_a + \psi_{fa}, \\ \psi_b = Li_b + \psi_{fb}, \\ \psi_c = Li_c + \psi_{fc}. \end{cases} \tag{2}$$

Here, L is the stator winding inductance; ψ_{fa}, ψ_{fb}, and ψ_{fc} are the flux linkages that the permanent magnet makes on the stator winding.

The stator voltage equations that PMSM works under the stationary α-β coordinates are

$$\begin{cases} L\dfrac{di_\alpha}{dt} = u_\alpha - e_\alpha - Ri_\alpha, \\ L\dfrac{di_\beta}{dt} = u_\beta - e_\beta - Ri_\beta. \end{cases} \tag{3}$$

The back EMF equations that PMSM works under the stationary $\alpha - \beta$ coordinates are

$$\begin{cases} e_\alpha = -\Psi_f \omega_r \sin\theta, \\ e_\beta = \Psi_f \omega_r \cos\theta. \end{cases} \tag{4}$$

Here, i_α, i_β, u_α, and u_β are the stator current and voltage of α - β axis; Ψ_f is the flux linkage of rotor permanent magnet; ω_r is the electrical angle speed of the rotor; θ is the electrical angle of the rotor.

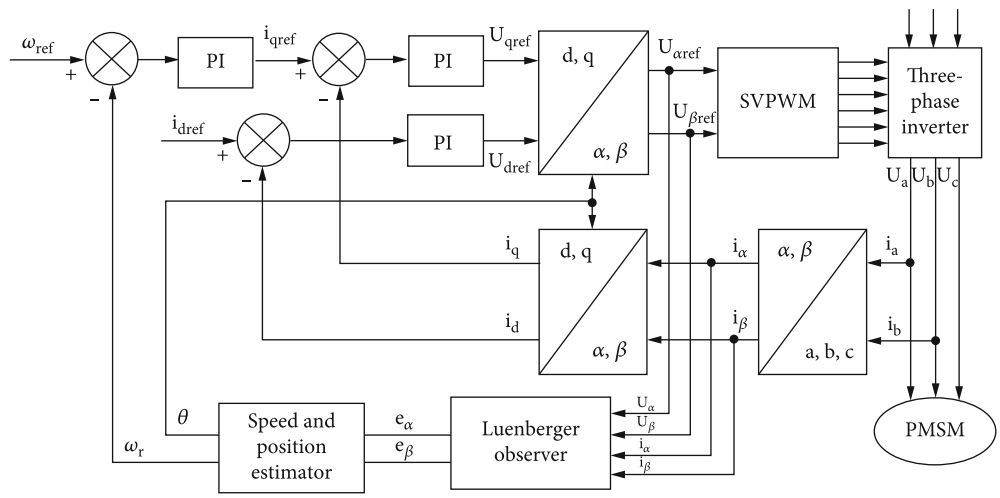

Figure 1: Block diagram of PMSM sensorless control system based on LO.

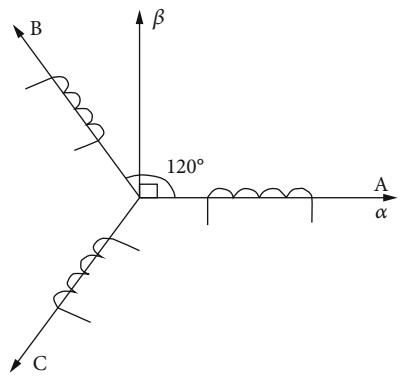

Figure 2: Stationary stator coordinate.

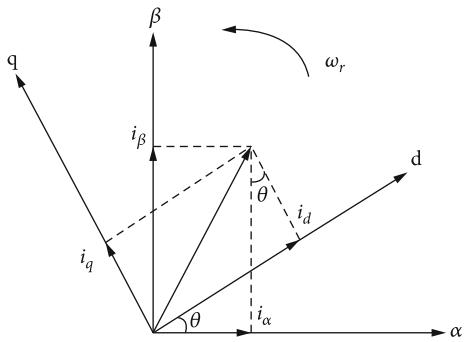

Figure 3: Vector diagram.

The voltage equations that PMSM works under d and q coordinates are as follows:

$$\begin{cases} u_d = Ri_d + \dfrac{d\psi_d}{dt} - \Psi_q \omega_r, \\ u_q = Ri_q + \dfrac{d\psi_q}{dt} - \Psi_d \omega_r, \end{cases} \tag{5}$$

where u_d and u_q are the stator voltage on the axis d and q, respectively, i_d and i_q are the stator current on the axis d and q, respectively, and ψ_d and ψ_q are the stator flux linkage component on the axis d and q, respectively.

The stator flux linkage component on the axis d and q can be described by

$$\begin{cases} \psi_d = \Psi_f + L_d i_d, \\ \psi_q = L_q i_q. \end{cases} \tag{6}$$

The equation of electromagnetic torque is

$$Te = \frac{3}{2} P\left[\Psi_f i_q + \left(\mathrm{L_d} - \mathrm{L_q}\right) i_\mathrm{d} i_q\right]. \tag{7}$$

Here, P is the pole-pairs number of the motor.

2.2. Mathematical Model of Luenberger Observer of PMSM. The basic structure of Luenberger observer is shown in Figure 4. According to the mathematical model of PMSM, we usually use the voltage and current of the PMSM, which could be measured easily, as the inputs to restructure its states. In Figure 4, a feedback control is introduced, and the feedback signal is the comparison of the estimated current with the actual one. It makes the estimated value be close to the actual value infinitely.

In Figure 4, i_α, i_β, u_α, and u_β are the stator current and voltage of α-β axis; $\widehat{i}_\alpha$ and $\widehat{i}_\beta$ are the estimated currents of α - β axis, respectively; $\widehat{e}_\alpha$ and $\widehat{e}_\beta$ are the estimated back EMFs of the α - β axis, respectively.

In the block diagram of Figure 4, $x = [e_\alpha \quad e_\beta]^T$, $u = [u_\alpha \quad u_\beta]^T$, and $y = [i_\alpha \quad i_\beta]^T$.

According to Figure 4, we can obtain the following equations:

$$\begin{cases} \dot{x} = Ax + Bu, \\ y = Cx, \end{cases} \tag{8}$$

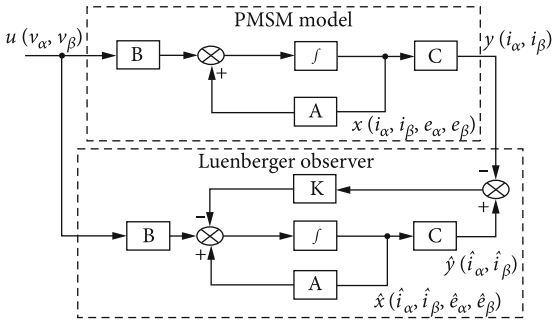

Figure 4: Basic structure of the traditional Luenberger observer.

$$\begin{cases} \dot{\hat{x}} = A\hat{x} + Bu - K(y - \hat{y}), \\ \hat{y} = C\hat{x}. \end{cases} \tag{9}$$

Substituting x, u, and y into equations (8) and (9), we can design the PMSM mathematical model of the Luenberger observer as follows:

$$\begin{cases} L\dfrac{d\hat{i}_\alpha}{dt} = u_\alpha - \hat{e}_\alpha - Ri_\alpha + K_{e1}\left(i_\alpha - \hat{i}_\alpha\right), \\ L\dfrac{d\hat{i}_\beta}{dt} = u_\beta - \hat{e}_\beta - Ri_\beta + K_{e1}\left(i_\beta - \hat{i}_\beta\right), \\ \begin{cases} \hat{e}_\alpha = -K_{e2}\left(i_\alpha - \hat{i}_\alpha\right), \\ \hat{e}_\beta = -K_{e2}\left(i_\beta - \hat{i}_\beta\right). \end{cases} \end{cases} \tag{10}$$

Here, K_{e1} and K_{e2} are the gains of the Luenberger observer.

After back EMF of Luenberger observer being estimated, the position angle of the rotor can be obtained directly by using the function below.

$$\hat{\theta}_e = \text{Arctan}\left(-\frac{\hat{e}_\alpha}{\hat{e}_\beta}\right). \tag{11}$$

Here, $\hat{\theta}_e$ refers to the estimated rotor electrical angle.

According to equations (4) and (11), the following function can be obtained.

$$\hat{\omega}_r = \frac{\sqrt{\hat{e}_\alpha{}^2 + \hat{e}_\beta{}^2}}{\Psi_f}. \tag{12}$$

Here, $\hat{\omega}_r$ refers to the estimated electrical angle speed.

According to equation (11), the arctangent function is used to calculate rotor electrical angle. In practice, there are lots of harmonics and noise in the control system due to the nonlinearity of the inverter. Therefore, the division operation in the arctangent function causes larger estimation error of rotor position and speed [19].

Another method for rotor position and speed estimation is using PLL, which can efficiently avoid the noise made by arctangent function, and the specific block diagram is shown in Figure 5 (we call this method as "2021 LO"). The whole control system is comprised of SVPWM, three-phase full bridge inverter circuit, Luenberger observer, and phase locked loop.

PLL is used to obtain the position and speed due to the excellent tracking performance on frequency and phase of PLL. The generic PLL block diagram is shown in Figure 6.

According to Figure 6, the following function can be obtained

$$\Delta \text{e} = -\hat{\text{e}}_a * \cos\left(\hat{\theta}\right) - \hat{\text{e}}_\beta * \sin\left(\hat{\theta}\right) = \Psi_f * \hat{\omega}_r * \sin\left(\hat{\theta}e - \hat{\theta}\right). \tag{13}$$

In Figure 6, $\hat{\omega}$ refers to the estimated rotor speed by the PLL, and $\hat{\theta}$ refers to the estimated rotor position angle by the PLL.

When $\hat{\theta}\text{e} - \hat{\theta} < \pi/8$, the following function can be used.

$$\sin\left(\hat{\theta}e - \hat{\theta}\right) \approx \hat{\theta}e - \hat{\theta}. \tag{14}$$

According to equation (14), Figure 6 can be equivalent to Figure 7.

According to Figure 7, the closed loop transfer function and error transfer function of phase locked loop can be obtained, respectively, as below:

$$G_1(s) = \frac{\hat{\theta}(s)}{\hat{\theta}\text{e(s)}} = \frac{\text{s}Kp + Ki}{s^2 + \text{s}Kp + Ki}, \tag{15}$$

$$G_2(s) = \frac{\Delta e(s)}{\hat{\theta}\text{e(s)}} = \frac{s^2}{s^2 + sKp + Ki}. \tag{16}$$

Here, $K = \Psi_f \hat{\omega}_r$. Since K is in the outside of the closed-loop system, it does not affect the stability of the PLL.

Since $K_p > 0, K_i > 0$, (15) and (16) are both minimum phase system. So, the stability of (15) and (16) is determined by their poles.

The characteristic equation of (15) and (16) is

$$s^2 + sKp + Ki = 0. \tag{17}$$

Hence, the poles of (15) and (16) are

$$s_{1,2} = \frac{-K_p \pm \sqrt{K_p^2 - 4K_i}}{2}. \tag{18}$$

Since $K_p > 0$ and $K_i > 0$, $s_{1,2} < 0$ if $K_p^2 - 4K_i > 0$, and the real parts of $s_{1,2}$ are negative if $K_p^2 - 4K_i > 0$.

Hence, for all $K_p > 0, K_i > 0$, (15) and (16) are stable.

As rotor position is a ramp function, the steady-state error of rotor position and speed estimation system by phase locked loop can be obtained as

$$\Delta\text{e}(\infty) = \lim_{s \longrightarrow 0} s * \Delta e(s) = \lim_{s \longrightarrow 0} \frac{\text{s}}{s^2 + sKp + Ki} = 0. \tag{19}$$

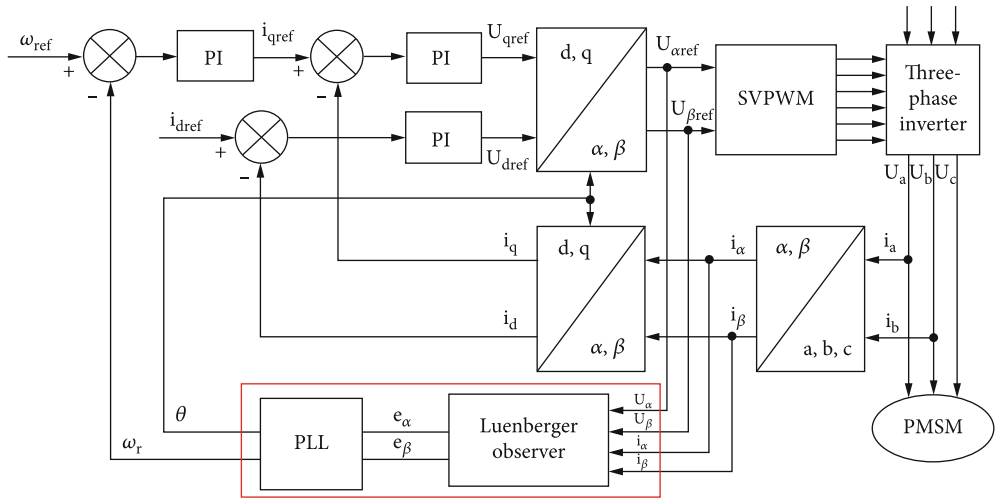

Figure 5: Block diagram of PMSM sensorless control system based on 2021 LO.

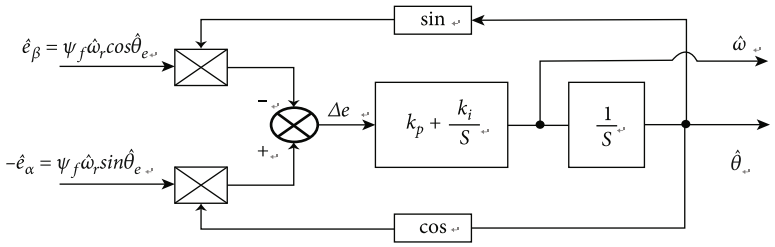

Figure 6: Block diagram of the PLL architecture.

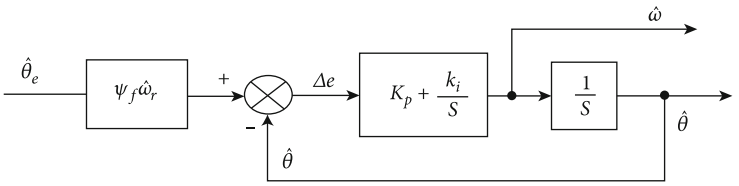

Figure 7: Equivalent diagram of the PLL.

Equation (19) shows that actual rotor position can be estimated by the PLL, and the PLL has a low pass filtering characteristic, which can perform secondary filtering on the back EMF to obtain the rotor position. Because the performance of phase-locked loop is determined by K_p and K_i, we found that it is very complex to calculate the value of K_p and K_i based on the analytical solution. In order to improve the estimating performance of position and speed, PSO can be used to optimize PI parameters of PLL and speed-loop in PMSM sensorless control system based on the 2021 LO. It can also improve estimated precision of position and speed and performance of dynamic response.

3. Optimizing PMSM Sensorless Control System

In practice, the load is often fluctuant when the PMSM is used, and it can cause maladjustment or overshooting of rotation speed if the parameters of PI controllers are not properly tuned. It is hard to meet the requirements in high precision rotation speed control. Hence, it is necessary to optimize the PI values of speed-loop in PMSM sensorless control system and improve the performance of speed control. The specific block diagram of the proposed system is shown in Figure 8. The following two subsections show how to apply PSO to the Luenberger observer-based PMSM sensorless control system.

3.1. Introduction of PSO. PSO was put forward by Oubelaid et al. [24]. The information of every particle in the particle swarm is iterated and updated constantly. In every iteration, it can calculate the optimal values of individual particle and all the particles (pbest and gbest). After calculating the pbest and gbest, every particle adjusts its flight speed and location. The formulas of speed and location updating of particles are

$$\begin{cases} u_{ij}(t+1) = u_{ij}(t) + c_1 r_1 \left[\text{pbest}_{ij}(t) - x_{ij}(t)\right] + c_2 r_2 \left[\text{gbest}_{ij}(t) - x_{ij}(t)\right], \\ x_{ij}(t+1) = x_{ij}(t) + u_{ij}(t). \end{cases} \tag{20}$$

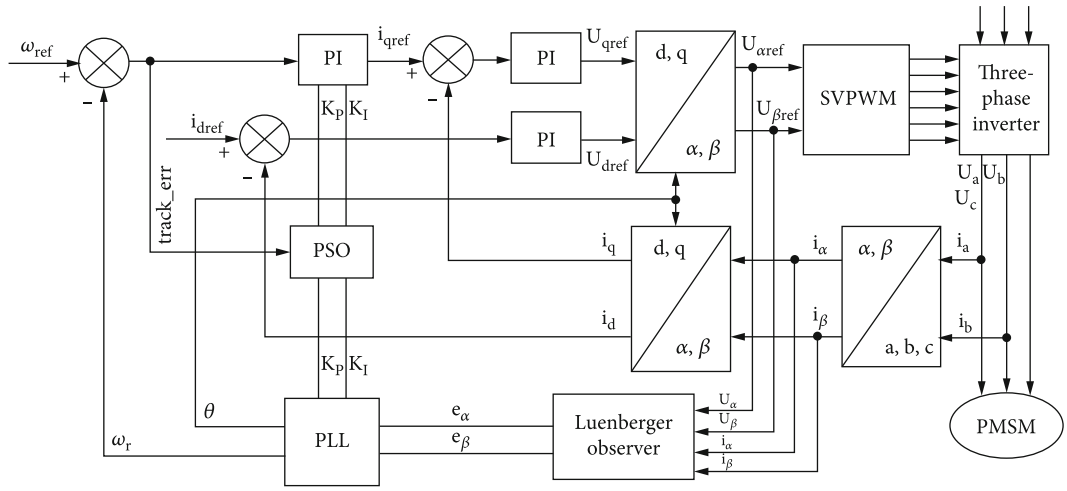

Figure 8: Block diagram of optimized PMSM sensorless control system by PSO.

In the equations, $u_{ij}(t)$ refers to velocity of particle i in j dimension after t times' iteration; $x_{ij}(t)$ refers to location of particle i in j dimension after t times' iteration; c_1 and c_2 are learning factors in particle swarm; r_1 and r_2 refer to two random numbers in (0, 1).

The topology of the particles plays important role for the optimization performance, and there are several kinds of topologies such as ring topology, global topology (also called full connection topology), and random topology (it is the default set of the standard PSO 2007 [25]). The ring topology means that each particle only has two fixed neighbors, the global topology is the above described one and its formula is (20), and the random topology means that the topology of particles are not fixed and is dynamically changed according to preset condition(s).

3.2. PSO-Based PMSM Sensorless Control System. In this paper, the optimization of the PI parameters of PLL and speed-loop is realized using the standard PSO 2007 [25]. Firstly, we need to select the objective function. In order to get a good control performance, the absolute value of speed difference between the target setting value and estimating value of observer should be small enough. The objective function is

$$|\text{Track\_err}(t)| = |\omega_t(t) - \widehat{\omega}_r(t)|. \tag{21}$$

Here, $\text{Track\_err}(t)$ is the speed difference between the target setting value and estimating value of observer at time t, and $\omega_t(t)$ is the target setting speed in time t.

In consideration of the system's tuning time should be small, we use the ITAE (integral time absolute error) as the evaluation function. Its continuous state function is (22), and its discrete state function is (23).

$$F_{\text{ITAE}} = \int_0^t \left|\text{Track}_{\text{err}(t)}\right| d(t). \tag{22}$$

Table 1: PMSM parameters.

Parameters	Values
Rated voltage	310VDC
Number of poles	8 poles
Phase resistance (Rs)	2.875 ohms
Phase inductance (Ls)	8.5 mH
Rotor flux linkages (Ψ_f)	0.175 Wb

Since the fixed-step solver ode3 is used to simulate the control system, we can use the following equation as the objective function which is similar to (22).

$$F = \sum_{i=0}^{n} |\text{Track\_err}(k)|. \tag{23}$$

The variables to be optimized include 4 parameters, K_p and K_i of PLL and K_p and K_i of speed-loop. We label them as PLL_K_p, PLL_K_i, n_K_p, and n_K_i.

4. Simulation of System and Experimental Verification

In order to verify the feasibility and performance of the proposed control system, simulations and experiments are carried out. The parameters of PMSM, PSO, the 2021 LO, and the LO are shown in Tables 1–4.

4.1. Construct Simulation Model. According to the above analysis, the simulation model of PSO-based PMSM sensorless control system is shown in Figure 9 realized in MATLAB/Simulink. The whole simulation model is comprised of PMSM, SVPWM, three-phase full bridge inverter circuit, Luenberger observer, phase locked loop, and PSO. Here, PSO is used to optimize the whole system by calling the simulation file.

Table 2: Parameters of PSO.

Parameters	Size	Iterations	C1 C2	Search space			
				PLL_K_p	PLL_K_i	n_K_p	n_K_i
Values	4	100	0.8	100-2000	10000-60000	0.2-5	0.1-10

Table 3: PI parameters of 2021 LO [26, 27].

Parameters	PLL_K_p	PLL_K_i	n_K_p	n_K_i
Values	500	2000	0.14	7

Table 4: PI parameters of LO [27].

Parameters	n_K_p	n_K_i
Values	0.14	7

4.2. Comparative Analysis of PSO with Different Topologies. The parameters of PMSM in this simulation are shown in Table 1. According to foregoing analysis, the PLL is stable when both the value of PLL_K_p and PLL_K_i are greater than zero, but the range is too big. According to theoretical estimation [26] and experience in engineering application [27], the variable search spaces and PSO parameter set are given in Table 2, and the flowchart of PSO algorithm optimization is given in Figure 10. The whole simulation time is 0.1 second, and the target speed is 1000 RPM. When the time is at 0.05 second, we increase the load to 2 Nm. After 98 iterations of PSO, we got the optimal parameters of PI shown in Table 5. Track_err is convergent and close to zero. The value of evaluation function is 3.7386e+06.

In order to find which topology can achieve better optimization performance, we did comparisons among the ring topology, global topology, and the standard PSO 2007 (random topology). In the same condition, we simulated 10 times for each topology, and the results are shown in Table 6. From Table 6, we can conclude that the ITAE of standard PSO 2007 (the random topology) is better or smaller than that of the PSO with ring topology and global topology, but the computational time of ring topology is better than standard PSO and global topology, since there are fewer neighbors and less comparisons for the ring topology.

4.3. Simulation and Analysis of PMSM Performance. According to the simulation result of Subsection 4.2, we used the optimal parameters of PI by standard PSO 2007 (shown in Table 5) to verify the quantitative performance of the proposed method. LO [23] and 2021 LO [2] are compared with the proposed method based on the simulations. In the simulations, the same PMSM model and same simulation conditions were used.

(1) Comparison of speed curve

The simulation results are shown in Figure 11. We can conclude that PSO has obvious advantages in speed dynamic performance.

(2) Comparison of control performance

The simulation comparisons are based on the maximum speed overshoot, transient time and ITAE, and they are shown in Table 7. From Table 7, we can conclude that the performance of PMSM has been improved significantly using the proposed method.

4.4. Comparative Analysis of Simulation Results of PMSM Sensorless Control System. According to the simulation results of Subsection 4.2, the PI parameters optimized by PSO were applied to the simulation model of PMSM sensorless control system. The performance of PMSM was compared with the LO and the 2021 LO. The simulation condition is same as Subsection 4.2.

Figures 12–14 show the back EMF waveforms using the LO, the 2021 LO and the proposed method, respectively. These waveforms are perfect sine waves of three back EMF. The start and operation processes of PMSM are quite stable, which build a good foundation for the accurate estimations of the rotor position and speed. This proves that there is no obvious difference on back EMF performances of these three observers under this simulation condition.

Figures 15–17 show the estimated position and the actual position waveforms for the LO, the 2021 LO, and the proposed method. From Figures 15–17, it can be found that the position angle deviation of proposed method between estimation and actual position is smaller than other two methods.

Figures 18–20 show the position estimation errors using the LO, the 2021 LO, and the proposed method, respectively. Comparing these waveforms, we can get the following:

(a) The position estimation errors of the LO, the 2021 LO, and the proposed method are 2.9° (about 0.051 rad), 2.18° (about 0.038 rad), and 1.58° (about 0.0275 rad), respectively, when start up

(b) The position estimation errors are 2.5° (about 0.0436 rad), 1.8° (about 0.0314 rad), and 1.2° (about 0.0209 rad), respectively, in steady state

It shows that the position estimation error of PMSM is smaller using the proposed method than that of other two methods.

Figures 21–23 show the estimated speed and actual speed about the LO, the 2021 LO, and the proposed method, respectively. It showed that compared with the proposed method, the speed overshoot of PMSM is bigger by using the LO and the 2021 LO, and the time from start to steady state is longer.

Figures 24–26 show the speed estimation error using the LO, the 2021 LO, and the proposed method, respectively.

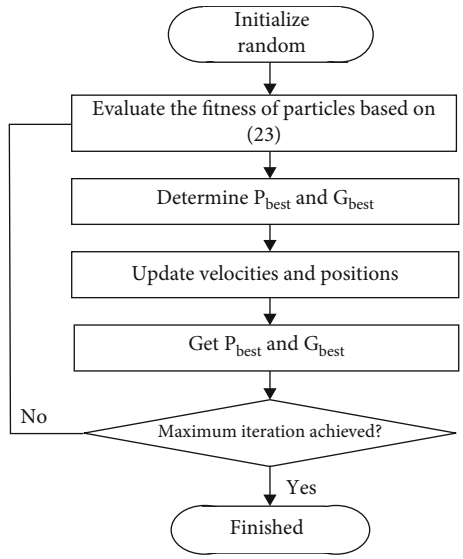

Figure 9: Simulink/MATLAB model of PSO-based PMSM sensorless control.

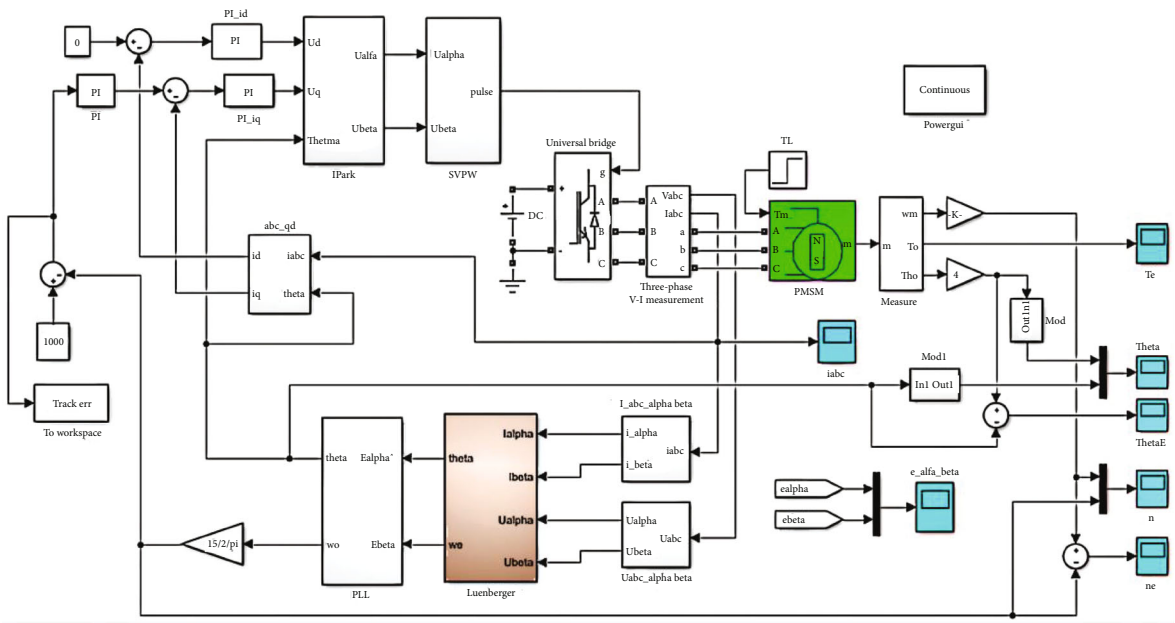

Figure 10: Flowchart for PSO algorithm optimization.

Table 5: PI parameters of proposed method.

Parameters	PLL_K_p	PLL_K_i	n_K_p	n_K_i
Values	1212	42970	0.5823	0.4127

Table 6: Comparison of standard PSO 2007 with different topologies.

Description	Ring topology	Standard PSO 2007	All topology
Min. ITAE	3.7345e+06	3.7349e+06	3.7367e+06
Max. ITAE	3.7651e+06	3.7464e+06	3.8265e+06
Mean ITAE	3.7426e+06	3.7412e+06	3.7548e+06
Mean computational time (s)	545.92	549.34	565.12

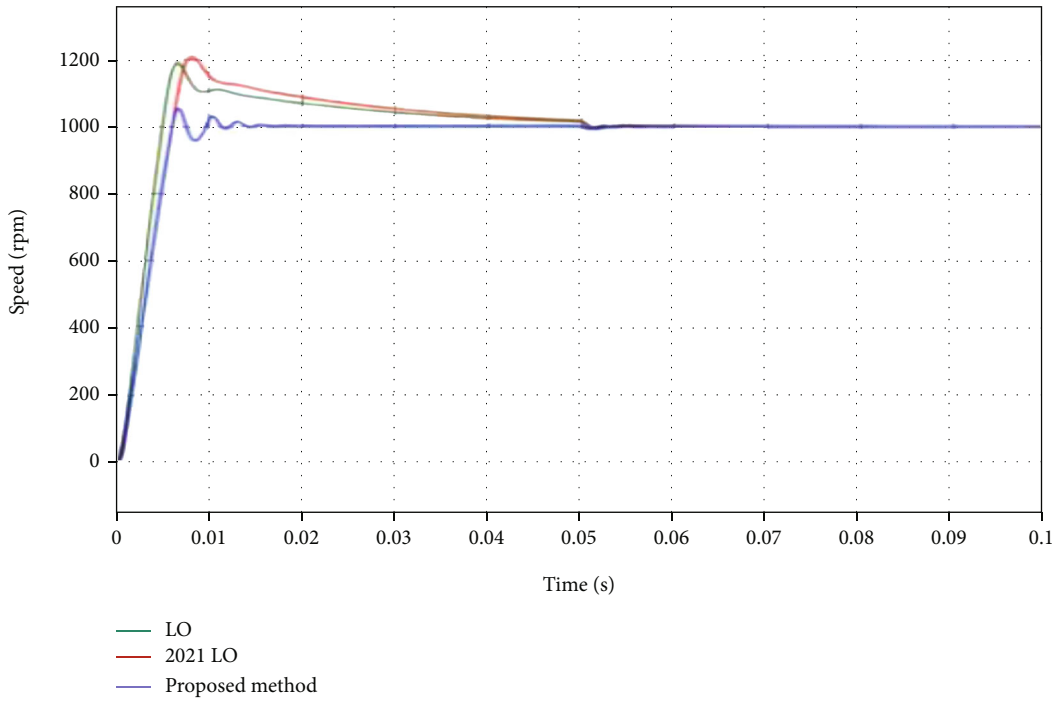

Figure 11: Comparison of speed curve.

Table 7: Comparison of optimization performance.

Type	Speed overshoot (%)	Transient time (ms)	ITAE
LO	18.8%	43	2.7648e+07
2021 LO	20.8%	42	6.6414e+06
Proposed method	5.3%	11	3.7386e+06

Speed overshoot = (max.speed overshoot/target setting speed − 1) ∗ 100%. Transient time: set the error is 2%.

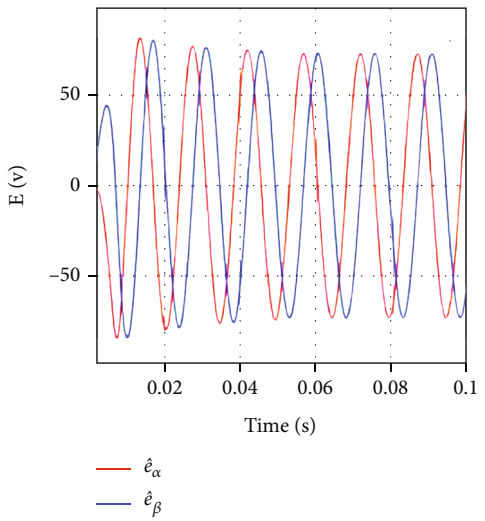

Figure 12: BEMF waveforms using the LO.

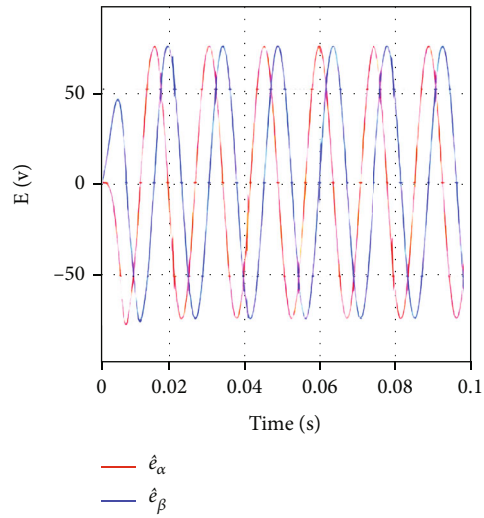

Figure 13: BEMF waveforms using 2021 LO.

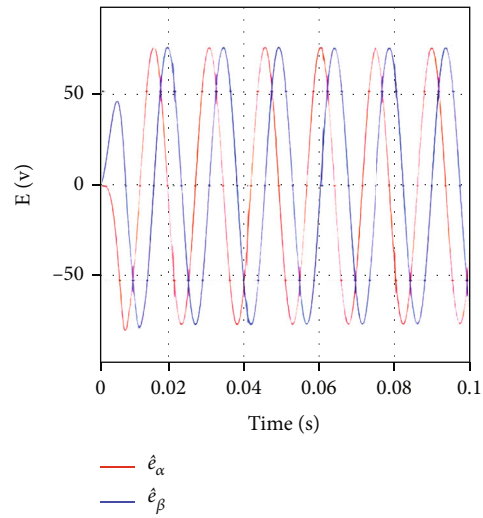

Figure 14: BEMF waveforms using the proposed method.

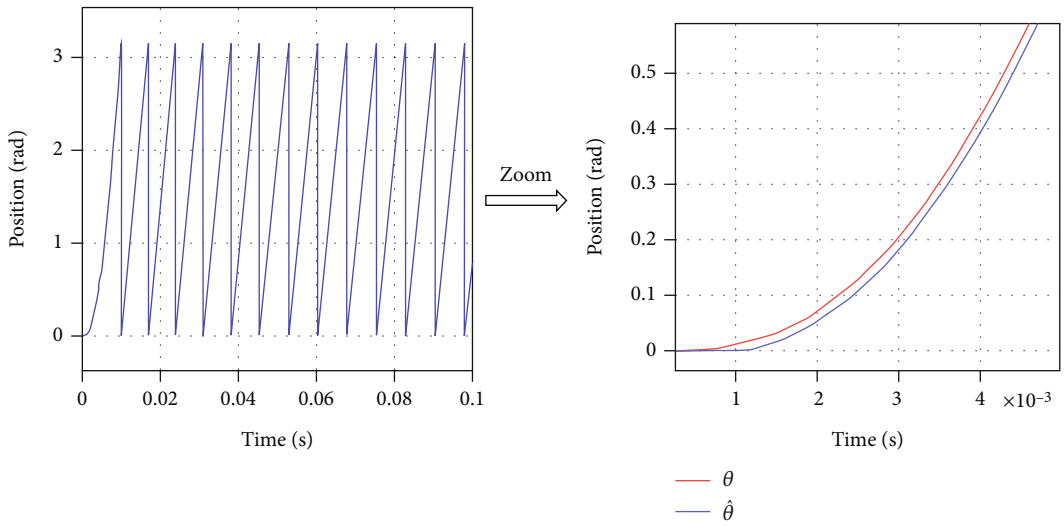

Figure 15: Results of estimated position using the LO.

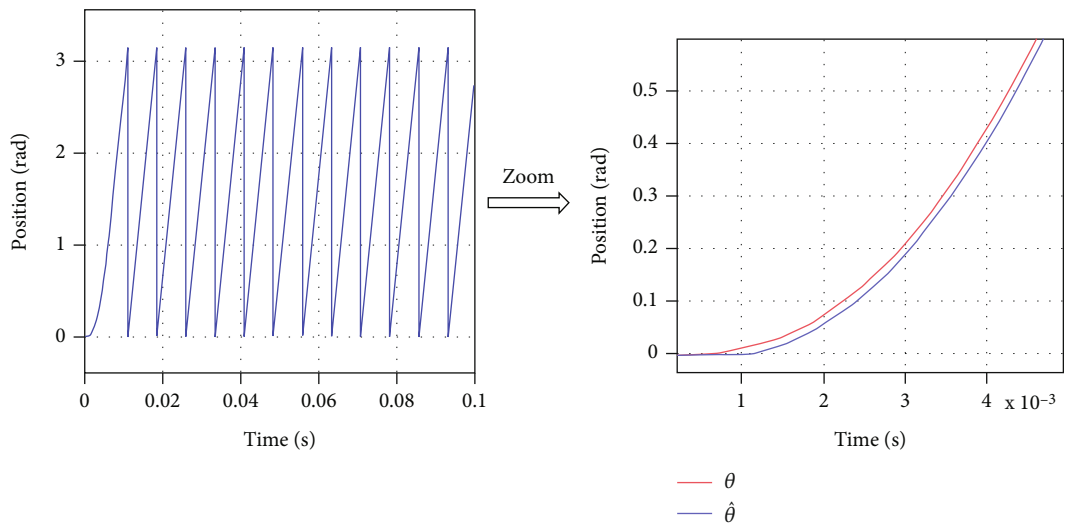

Figure 16: Results of estimated position using the 2021 LO.

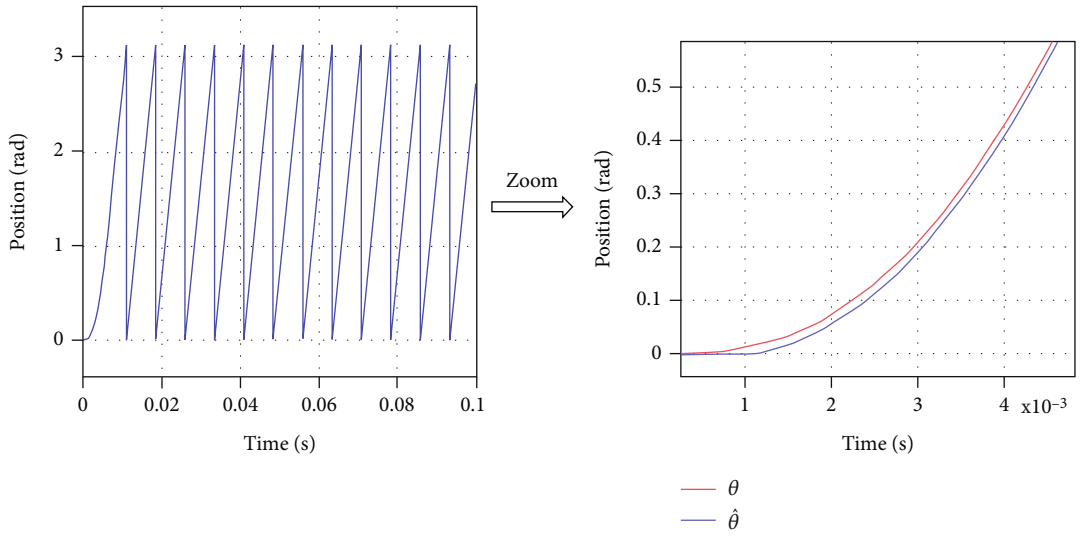

Figure 17: Results of estimated position using the proposed method.

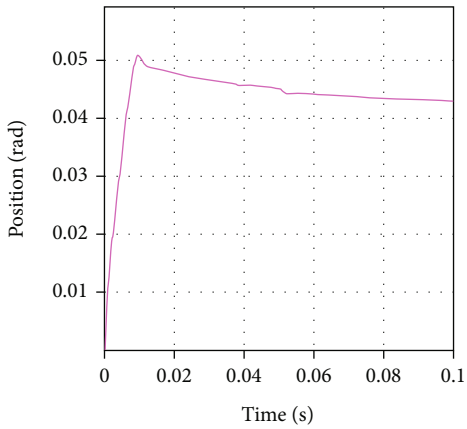

Figure 18: Position estimation errors using LO.

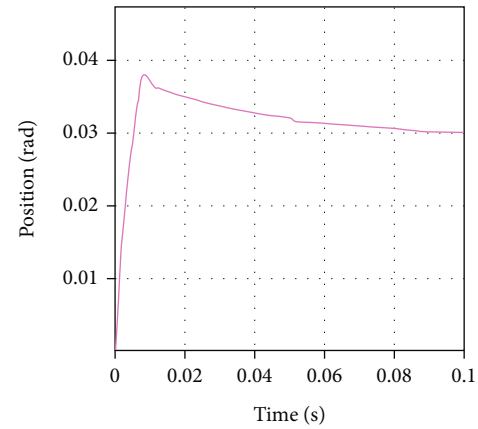

Figure 19: Position estimation errors using 2021 LO.

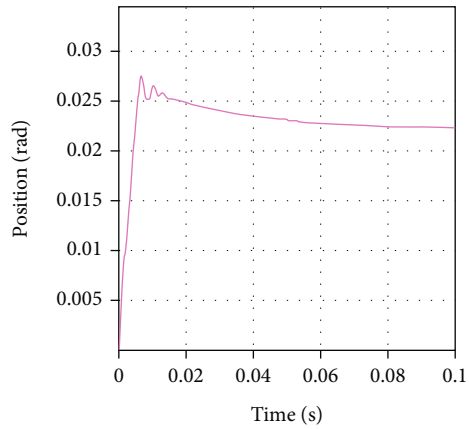

Figure 20: Position estimation errors using proposed method.

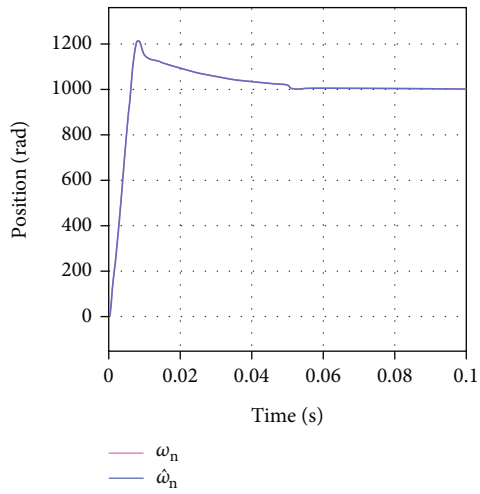

Figure 21: Estimated speed and actual speed for LO.

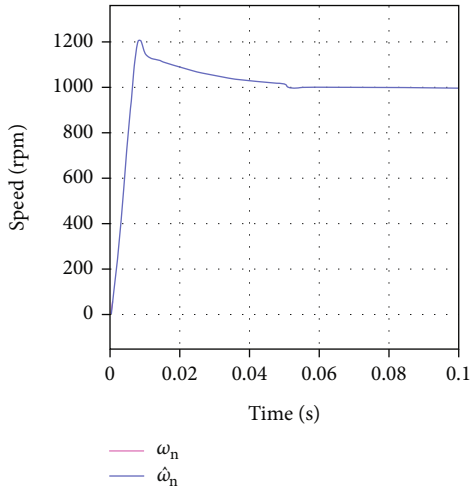

Figure 22: Estimated speed and actual speed for 2021 LO.

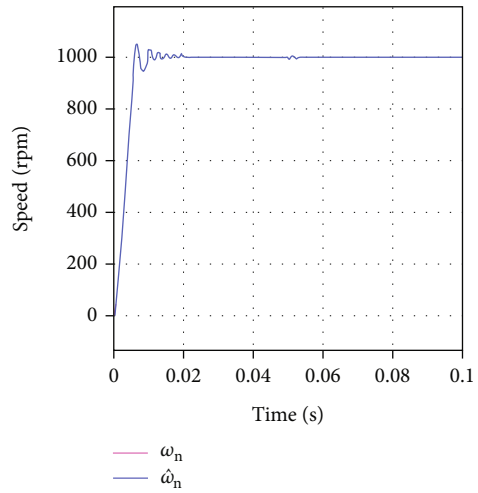

Figure 23: Estimated speed and actual speed for proposed method.

Comparing these waveforms, it shows that the proposed method is better than the LO and the 2021 LO of the error of speed estimation when start-up, and the speed error is about ±0.1 RPM when in steady state.

Table 8 lists the simulation data on the accuracy of estimated position and estimated speed, and it can be found that the proposed method can achieve better performance than other two methods.

4.5. Robustness Analysis of PMSM Sensorless Control Based on Simulations. In practice, the robustness is important for a control system. In order to verify the robustness of the optimized PMSM system, the work performance on no-load and full-load is to be verified based on two cases.

Case 1. The whole simulation time is 0.1 second. Firstly, we set the PMSM running at 1000 RPM without load, and then, the 2 Nm load is applied to the system at $t = 0.05$ second. The simulation results are shown in Figure 26, which shows the waveform of speed appeared fluctuations, but it goes stably immediately.

Case 2. The whole simulation time is 0.1 second. Firstly, we set the PMSM running at the 1000 RPM with full load 2 Nm. When $t = 0.05$ second, the load and speed are changed to 1 Nm (50% of load torque changes) and 500 RPM (50% of speed changes), respectively. Simulation results of speed and speed estimation error are shown in Figures 27 and 28, respectively. The simulation results showed that the speed fluctuates slightly and then be stabilized quickly when the speed and torque are changed.

According to the simulation results above, it proves that the control system has good robustness and dynamic response.

4.6. Experimental Results and Analysis. It is important to verify the proposed PSO optimization method using physical system. Here, using STM32F030 MCU as its main control chip and writing the software code in C language, a PMSM sensorless control system is designed. The

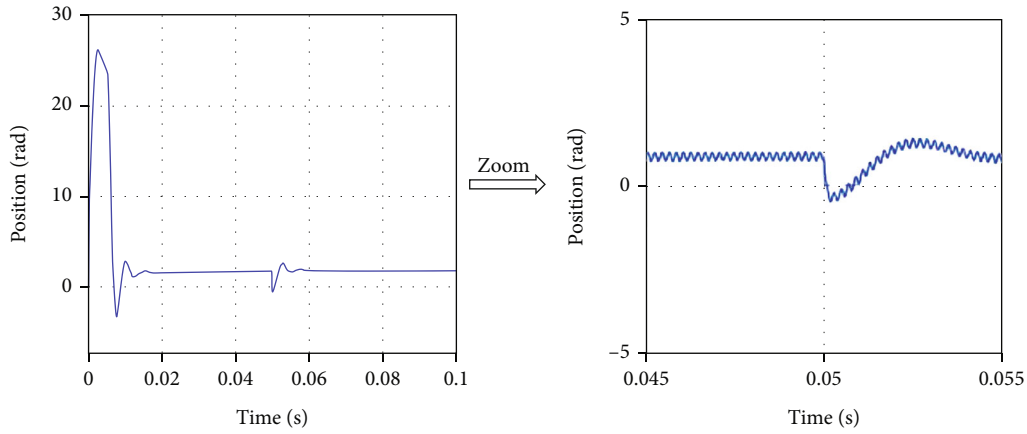

Figure 24: Speed estimation error using the LO.

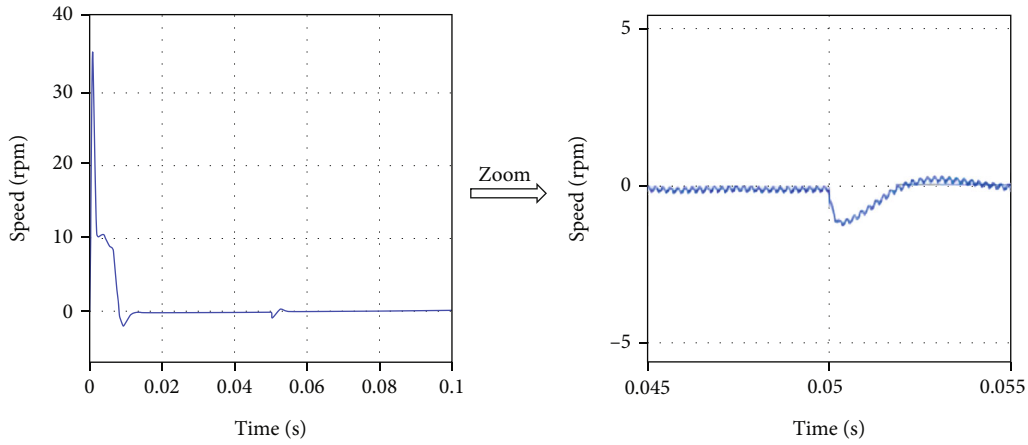

Figure 25: Speed estimation error using the 2021 LO.

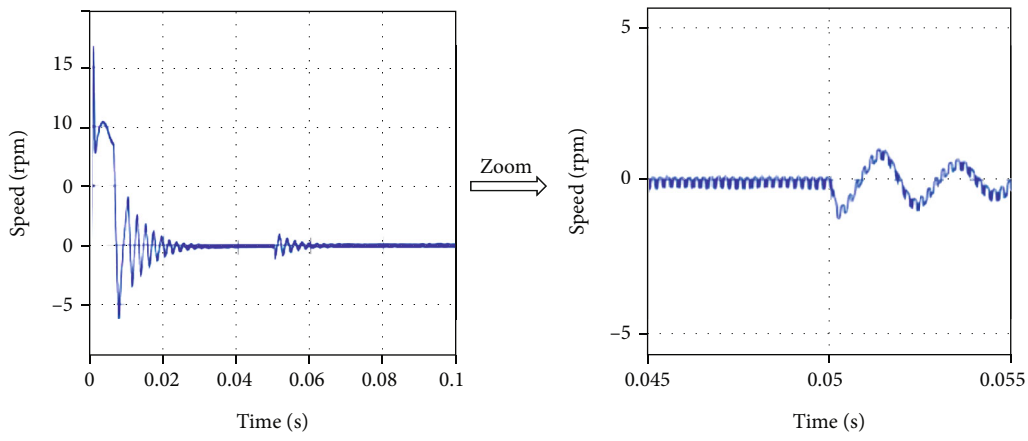

Figure 26: Speed estimation error using the proposed method.

parameters of PMSM are same as Table 1. Experimental platform is shown in Figure 29.

In order to verify the accuracy of speed, 2 Nm loads are applied to the PMSM by hysteresis dynamometer when speed running at 1000 RPM, and the phase current waveform, torque, and speed are shown in Figure 30. The waveforms show that the phase current presents a perfect sine wave, and the motor speed is stabilized at about 1000.05 RPM. It shows that the speed results of experiment are consistent with the simulation results.

To verify the robustness of optimized PMSM system, two experimental cases are carried out.

Table 8: Performance comparison of PMSM sensorless control system.

Item	Description	LO	2021 LO	Proposed method
1	Error for estimated position and actual position when start up	2.9°	2.18°	1.58°
2	Error for estimated position and actual position at stable running	2.5°	1.8°	1.2°
3	Error for estimated speed and actual speed when start up	27 RPM	35 RPM	17 RPM
4	Error for estimated speed and actual speed at stable running	±1 RPM	±0.1 RPM	±0.1 RPM

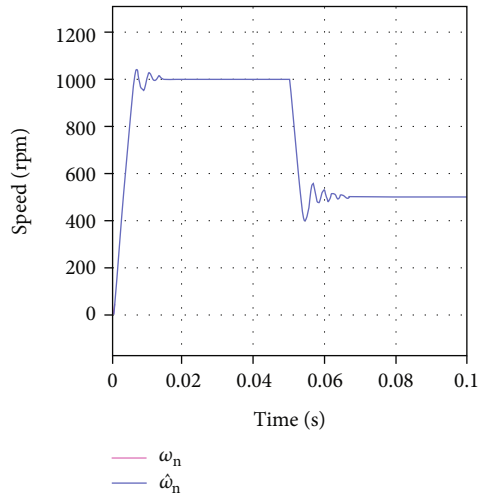

Figure 27: Estimated speed and actual speed for proposed method at Case 2.

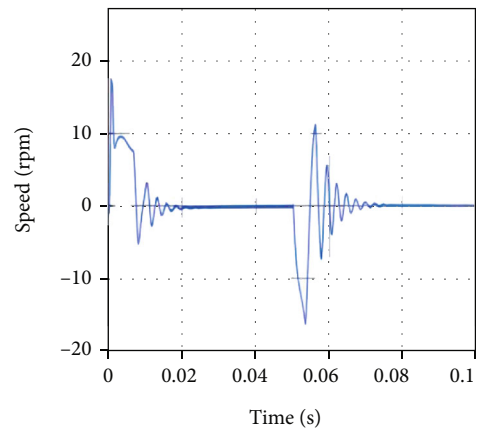

Figure 28: Speed estimation error for proposed method at Case 2.

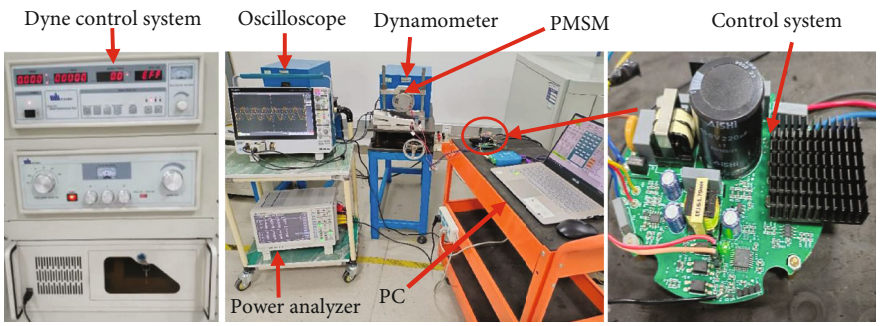

Figure 29: Experimental installation.

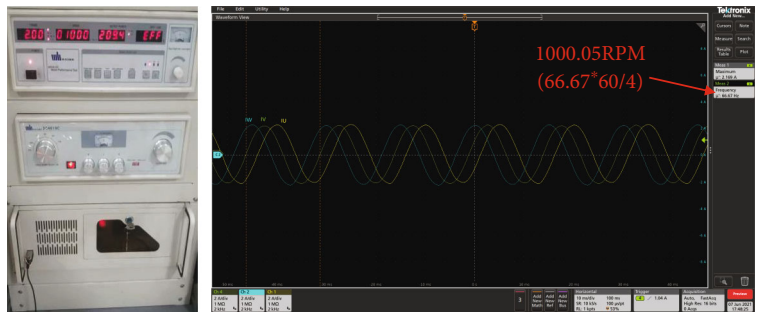

Figure 30: Phase current waveform, torque, and speed measurement for proposed method.

Figure 31: Phase current waveform for proposed method.

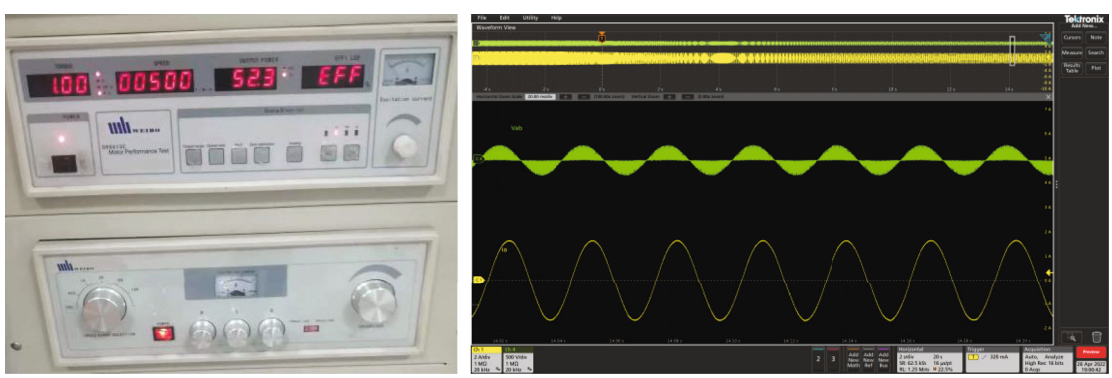

Figure 32: Phase current waveform, torque, and speed measurement for proposed method.

Case 1. In order to verify the robustness of the PMSM physical system, 2 Nm loads are applied to PMSM by hysteresis dynamometer after the speed stabilizes at 1000 RPM without load, and the test data is shown in Figure 31. These phase currents are perfect sine waves. The current changes very smoothly, without abnormal fluctuations when the load is applied to the PMSM system.

Case 2. In order to verify the robustness of PMSM physical system under full load condition, the load and speed are changed to 1 Nm and 500 RPM, respectively, after PMSM system becomes stable with a speed of 1000 RPM and a 2 Nm load. The test data is shown in Figure 32. The waveform shows that the current changes very smoothly, without abnormal fluctuations when the test condition changes.

According to the above experiments, it proves that experimental results are consistent with the simulation results, and the optimized PMSM system has good stability and robustness. Because of the limited resources, the rotor position angle and speed overshoot are not obtained in the experiment. According to equations (4) and (13), the speed is proportional to the position angle. Combined with the

speed testing data above, it can be deduced that the position angle is consistent to the simulation data.

5. Conclusion

This paper proposed to use the PSO algorithm to optimize the PI parameters of PLL and the speed-loop of the Luenberger observer-based PMSM sensorless control system. The simulation results in MATLAB/Simulink showed that the PSO algorithm can reduce the parameter tuning difficulty of PLL and speed loop effectively. Then, we applied the optimized PI parameters to the Simulink model of PMSM sensorless control system and physical system. The simulation results and experimental results showed that the proposed method can improve performance of position estimation and speed estimation. Moreover, the PSO with different topologies was tested, and it was found that the random topology of PSO can achieve better performance than the ring topology and global topology. Finally, simulations and experiments have been used to verify the robustness of the proposed method, and the results show that the optimized system has good performance when there are uncertainties or disturbances. Since the system model is based on MATLAB/Simulink, it is difficult to convert it to the codes, which can be run in the microcontroller of the experimental system. In the future, we will simplify the system model and the PSO algorithm, so the proposed method can real-time tune the system parameters.

Abbreviations

PMSM: Permanent magnet synchronous motor
PSO: Particle swarm optimization
PI: Proportional–integral
PLL: Phase locked loop
LO: Luenberger observer
FOC: Field-oriented control
HFI: High-frequency injection
MRAS: Model reference adaptive system
FLO: Flux linkage observer
EKF: Extended Kalman filter
SMO: Sliding mode observer
SVPWM: Space vector pulse width modulation
EMF: Electromotive force
ITAE: Integral time absolute error.

Data Availability

No data were used to support this study.

Conflicts of Interest

The author declares that they have no conflicts of interest.

Acknowledgments

This research is supported partially by the South African National Research Foundation Grants (Nos. 141951, 132159, 137951, and 132797).

References

[1] Y. Zhu, B. Tao, M. Xiao, G. Yang, X. Zhang, and K. Lu, "Luenberger position observer based on deadbeat-current predictive control for sensorless PMSM," *Electronics*, vol. 9, no. 8, p. 1325, 2020.

[2] Q. Mi and R. Ma, "A novel Luenberger observer for the sensorless speed control of PMSM," in *In Proceedings of PCIM Asia 2021, International Exhibition and Conference for Power Electronics*, pp. 158–164, Shenzhen, China, Sep 2021.

[3] A. M. O. Anwer, F. A. Omar, and A. A. Kulaksiz, "Design of a fuzzy logic-based MPPT controller for a PV system employing sensorless control of MRAS-based PMSM," *International Journal of Control, Automation and Systems*, vol. 18, no. 11, pp. 2788–2797, 2020.

[4] C. Lascu and G.-D. Andreescu, "PLL position and speed observer with integrated current observer for sensorless PMSM drives," *IEEE Transactions on Industrial Electronics*, vol. 67, no. 7, pp. 5990–5999, 2020.

[5] J.-H. Jang, S.-K. Sul, H. Jung-IK et al., "Sensorless drive of surface-mounted permanent-magnet motor by high-frequency signal injection based on magnetic saliency," *IEEE Transactions on Industry Applications*, vol. 39, no. 4, pp. 1031–1039, 2003.

[6] K. Jung-Ik Ha, T. S. Ide, and S.-K. Sul, "Sensorless rotor position estimation of an interior permanent-magnet motor from initial states," *IEEE Transactions on Industry Applications*, vol. 39, no. 3, pp. 761–767, 2003.

[7] X. Luo, Q. Tang, A. Shen, and Q. Zhang, "PMSM sensorless control by injecting HF pulsating carrier signal into estimated fixed-frequency rotating reference frame," *IEEE Transactions on Industry Applications*, vol. 63, no. 4, pp. 2294–2303, 2016.

[8] A. H. Almarhoon, Z. Q. Zhu, and P. L. Xu, "Improved pulsating signal injection using zero-sequence carrier voltage for sensorless control of dual three-phase PMSM," *IEEE Transactions on Energy Conversion*, vol. 32, no. 2, pp. 436–446, 2017.

[9] N. K. Quang, N. T. Hieu, and Q. P. Ha, "FPGA-based sensorless PMSM speed control using reduced-order extended Kalman filters," *IEEE Transactions on Industrial Electronics*, vol. 61, no. 12, pp. 6574–6582, 2014.

[10] A. V. Ravi Teja, V. Verma, and C. Chakraborty, "A new formulation of reactive-power-based model reference adaptive system for sensorless induction motor drive," *IEEE Transactions on Industrial Electronics*, vol. 62, no. 11, pp. 6797–6808, 2015.

[11] S. Das, R. Kumar, and A. Bhaumik, "Speed sensorless model predictive current control of doubly-fed induction machine drive using model reference adaptive system," *ISA Transactions*, vol. 86, pp. 215–226, 2019.

[12] I. Benlaloui, S. Drid, L. Chrifi-Alaoui, and M. Ouriagli, "Implementation of a new MRAS speed sensorless vector control of induction machine," *IEEE Transactions on Energy Conversion*, vol. 30, no. 2, pp. 588–595, 2015.

[13] A. Choudhury, P. Pillay, and S. S. Williamson, "Modified stator flux estimation based direct torque controlled PMSM drive for hybrid electric vehicle," in *In Proceedings of 38th Annual Conference on IEEE Industrial Electronics Society*, pp. 2965–2970, Montreal, Canada, Oct 2012.

[14] W. Xu, Y. Jiang, C. Mu, and F. Blaabjerg, "Improved nonlinear flux observer-based second-order SOIFO for PMSM sensorless control," *IEEE Transactions on Power Electronics*, vol. 34, no. 1, pp. 565–579, 2019.

[15] A. Qiu, W. Bin, and H. Kojori, "Sensorless control of permanent magnet synchronous motor using extended Kalman filter," in *In Proceedings of Canadian Conference on Electrical and Computer Engineering*, pp. 1557–1562, Niagara Falls, Canada, 2004.

[16] A. Ahmad, H. Mickael, and D. Demba, "A sensorless PMSM drive using a two stage extended Kalman estimator," in *In Proceedings of the 34th Annual Conference of IEEE Industrial Electronics Society IECON*, pp. 1729–1734, Orlando, 2008.

[17] Z. Qiao, T. Shi, Y. Wang, Y. Yan, C. Xia, and X. He, "New sliding-mode observer for position sensorless control of permanent-magnet synchronous motor," *IEEE Transactions on Industrial Electronics*, vol. 60, no. 2, pp. 710–719, 2013.

[18] D. Liang, J. Li, R. Qu, and W. Kong, "Adaptive second-order sliding-mode observer for PMSM sensorless control considering VSI nonlinearity," *IEEE Transactions on Power Electronics*, vol. 33, no. 10, pp. 8994–9004, 2018.

[19] X. Song, J. Fang, B. Han, and S. Zheng, "Adaptive compensation method for high-speed surface PMSM sensorless drives of EMF-based position estimation error," *IEEE Transactions on Power Electronics*, vol. 31, no. 2, pp. 1438–1449, 2016.

[20] H. Jiacai, L. Hongsheng, and Q. Xu, "Senorless vector control of PMSM using sliding mode observer and fractional-order phase-locked loop," in *In Proceedings of the 31st Chinese Control Conference*, pp. 648–655, Hefei, China, July 2012.

[21] L. He, F. Wang, J. Wang, and J. Rodriguez, "Zynq implemented Luenberger disturbance observer based predictive control scheme for PMSM drives," *IEEE Transactions on Power Electronics*, vol. 35, no. 2, pp. 1770–1778, 2020.

[22] N. Henwood, J. Malaizé, and L. Praly, "A robust nonlinear Luenberger observer for the sensorless control of SM-PMSM: rotor position and magnets flux estimation," in *Proceedings of 38th Annual Conference on IEEE Industrial Electronics Society*, pp. 1625–1630, IECON, Montreal, QC, Canada, 2012.

[23] Z. Shuangfei, H. Haibo, and J. Wei, "Research on application of Luenberger observer in sensorless control of permanent magnet synchronous motor," *Electric Machines & Control Application*, vol. 44, no. 10, pp. 59–66, 2017.

[24] A. Oubelaid, Y. Berkani, N. Taib, and T. Rekioua, "Speed control and performance analysis of PMSM using particle swarm Optimization," in *Proceedings of international Conference on Applied Automation and Industrial Diagnostics*, pp. 1–9, DJELFA, Algeria, 2017.

[25] "Standard particle swarm optimization," http://particleswarm.info/Programs.html, May 2011.

[26] M. Preindl and E. Schaltz, "Sensorless model predictive direct current control using novel second-order PLL observer for PMSM drive systems," *IEEE Transactions on Industrial Electronics*, vol. 58, no. 9, pp. 4087–4095, 2011.

[27] Z. Rui, X. Xinhong, C. Lianbo et al., "Design of PI controller for PMSM using chaos particle swarm optimization algorithm," in *In Proceedings of International Conference on Mechatronics and Mechanical Engineering*, pp. 1–6, Wuhan, China, 2020.